# Nitrite-Induced Oxidation of Organic Coatings on Models for Airborne Particles[†]

**Federico Karagulian, Christopher W. Dilbeck, and Barbara J. Finlayson-Pitts***

*Department of Chemistry, University of California, Irvine, Irvine, California 92697-2025*

*Received: September 22, 2008; Revised Manuscript Received: December 3, 2008*

The UV photolysis at $\lambda \geq 290$ nm in air of a mixture of $NaNO_2$/NaCl coated with 1-oleoyl-2-palmitoyl-*sn*-glycero-3-phosphocholine (OPPC) was followed in real time in the absence and presence of water vapor by using diffuse reflection infrared Fourier transform spectroscopy (DRIFTS) at 23 °C. Matrix-assisted laser desorption/ionization mass spectrometry (MALDI-MS) was used to confirm the identification of the products. Photolysis of $NO_2^-$ is known to generate $O^-$, which in the presence of water forms OH + $OH^-$. Irradiation of the OPPC/$NaNO_2$/NaCl mixture led to a loss of nitrite and the formation of organic nitrates and carbonyl compounds. In the absence of added water vapor, carboxylate ions were also formed. These products are due to oxidation of OPPC by $O^-$ and OH radicals. The organic products formed per calculated $O^-$/OH generated by photolysis increased with relative humidity, consistent with a competition between OPPC and $NO_2^-$ for OH. This suggests a new mechanism of oxidation of organics on particles and on surfaces in air that have nitrite ions available for photolysis. Similar chemistry is likely to occur for nitrate ions, which also photolyze to generate $O^-$.

## Introduction

The hydroxyl radical is known to be one of the most reactive atmospheric oxidants, and it determines the lifetime of many compounds in the troposphere.[1] Although there are multiple known sources of OH in the atmosphere, some studies have shown that the photolysis of nitrite and nitrate ions can be important sources in the aqueous phase, including the quasiliquid layer on ice.[2−16] Nitrite ion has much larger absorption cross sections than nitrate ion in the region 300−400 nm. In addition, the nitrite absorption is shifted to longer wavelengths[17] where the intensity of available solar radiation is higher.

The nitrite ion is an intermediate in the conversion of NO and $NO_2$ into other oxides of nitrogen in the atmosphere. For example, on thin aqueous surface films $NO_2$ undergoes heterogeneous hydrolysis to generate HONO and $HNO_3$ (see ref 18 and references therein):

$$2NO_2 + H_2O \rightarrow HONO + HNO_3 \quad (1)$$

While most of the HONO is released into the gas phase, some remains on the surface,[19,20] part of which may be in the form of nitrite ion.

Nitrite ion formation in air is also associated with sea salt chemistry. Wave action generates airborne sea salt particles,[21,22] and as they are transported, the components NaCl and NaBr react with various oxides of nitrogen[23,24] such as $NO_2$, $HNO_3$, $N_2O_5$, and $ClONO_2$. In the case of $NO_2$, gaseous ClNO is formed,[23,25,26] which can hydrolyze to form nitrite ions. In addition, all of these reactions with oxides of nitrogen convert the halide ions into photochemically active halogen gases, leaving behind nitrate ion, which in turn photolyzes to form, in part, $NO_2^-$:[17,27−29]

$$NO_3^- + h\nu\ (<350\ \text{nm}) \rightarrow NO_2 + O^- \quad (2a)$$

$$\rightarrow NO_2^- + O(^3P) \quad (2b)$$

In the presence of water, the $O^-$ generated in reaction 2a reacts to form the highly reactive OH free radical:[27,30]

$$O^- + H_2O \rightarrow OH + OH^- \quad (3)$$

The photolysis of nitrite ions also generates $O^-$ and hence OH:[2,7,8,17,28,29,31−34]

$$NO_2^- + h\nu \xrightarrow{k_p} NO + O^- \quad (290 \leq \lambda \leq 400\ \text{nm}) \quad (4)$$

Both nitrite and nitrate ions have been observed in upwelling areas of the ocean and their photolysis is proposed to be a significant source of aqueous OH through the above reactions.[35,36]

Oxidation of organic compounds in the lower atmosphere drives a variety of atmospherically relevant processes, from the formation of ozone to secondary organic aerosol (SOA).[1,37−39] While a great deal is known about gas phase oxidations, e.g., by OH radicals, very little is known about such processes for organics adsorbed on surfaces, which are ubiquitous in the troposphere. In the absence of other information, it is generally assumed that oxidation of these surface-bound organics occurs from the "top down" via the uptake and further reaction of oxidants such as $O_3$ and OH.[1,40,41] Since sea salt particles contain surface-adsorbed organics,[41−48] OH generated by nitrate and nitrite photolysis in and on particles could react with the marine organics, leading to oxidation from the "bottom up". Another circumstance in which such photochemical oxidations may be important is in the Arctic and Antarctic snowpacks where very active photochemistry, believed to be at least in part due to nitrate and nitrite ions, forms a variety of oxides of nitrogen and leads to the generation of organic oxidation products such as HCHO.[9,49,50]

Previous studies in this laboratory[51−55] have shown that unsaturated phospholipids in a number of forms, including thin

[†] Part of the "Robert Benny Gerber Festschrift".

* Author to whom correspondence should be addressed. E-mail: bjfinlay@uci.edu. Phone: (949) 824-7670. Fax: (949) 824-2420.

10.1021/jp808419g CCC: $40.75 
Published on Web 01/13/2009

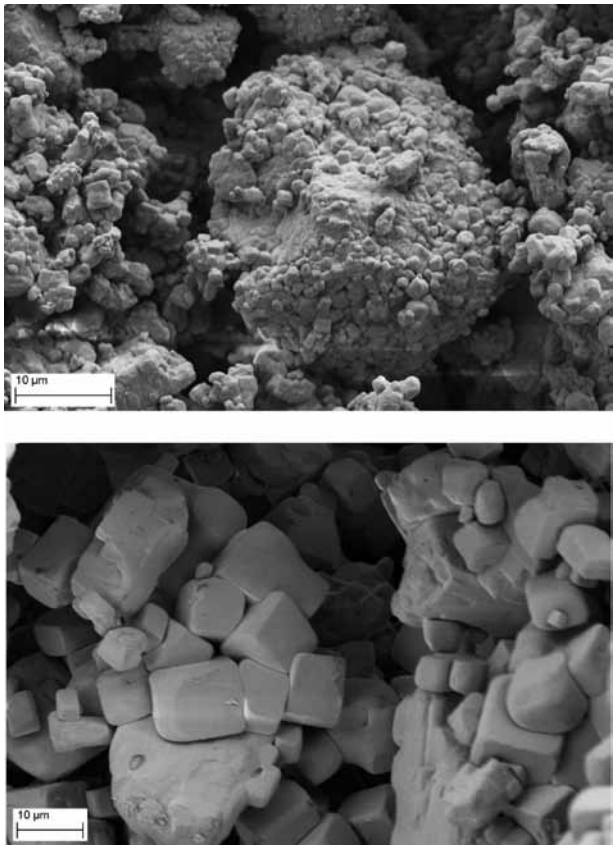


**Figure 1.** SEM images of OPPC/$NaNO_2$/NaCl (top) (0.4% w/w $NaNO_2$/NaCl) and OPPC/NaCl (bottom). In both cases, the OPPC would be ~1 monolayer if evenly distributed over the salt.

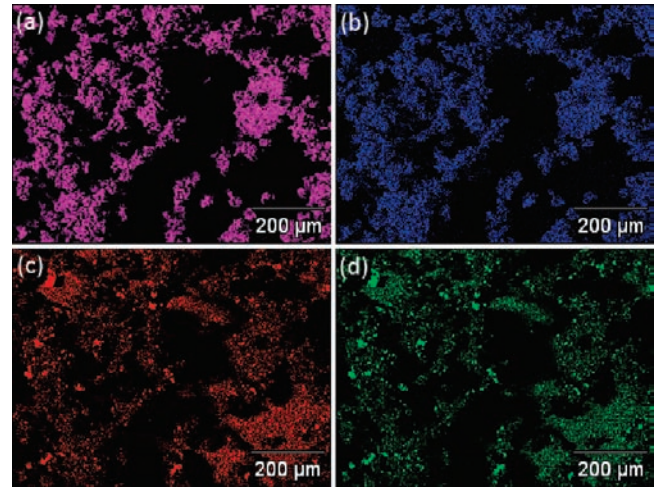


**Figure 2.** Element maps indicating location of (a) Na, (b) Cl, (c) N, and (d) O in a 5% $NaNO_2$/NaCl mixture.

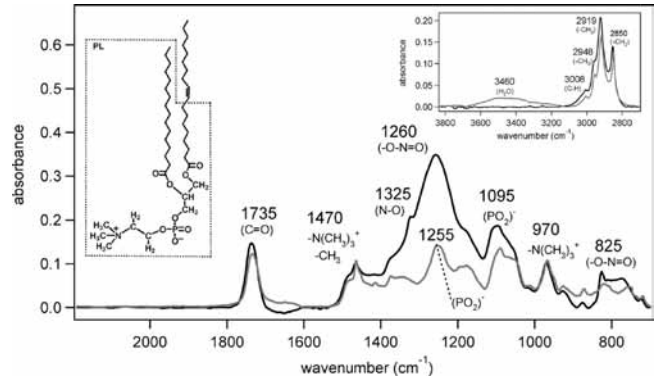


**Figure 3.** DRIFTS spectrum of a 0.4% w/w $NaNO_2$/NaCl mixture coated with ~1 ML of OPPC (OPPC/$NaNO_2$/NaCl, black line). The gray line is the DRIFTS spectrum of NaCl coated with ~1 ML of OPPC (OPPC/NaCl). The spectra were baseline corrected. The *y* axis is $\log(S_1/S_2)$, where $S_1$ is the single beam spectrum of NaCl alone and $S_2$ is the single beam spectrum of OPPC/$NaNO_2$/NaCl or OPPC/NaCl at ~ 0% RH, respectively. The inset on the left shows the structure of OPPC. "PL" is used throughout the text to denote the portion of the molecule enclosed within the dotted line.

films, either adsorbed on NaCl as a model for sea salt or as a monolayer on water, are readily oxidized by gas phase $O_3$ from the "top down" to generate secondary ozonides and a number of other products. Recently, we reported initial studies showing that an unsaturated phospholipid can also be oxidized from the "bottom up" by OH generated during the photolysis of nitrite ion at 52% relative humidity in a $NaNO_2$/NaCl salt mixture upon which the organic is adsorbed.[56] Reported here are more extensive studies of the oxidation of 1-oleoyl-2-palmitoyl-*sn*-glycero-3-phosphocholine (OPPC) during nitrite ion photolysis over a range of water vapor concentrations. Interestingly, there is a change in products and mechanism under dry conditions compared to those in the presence of water vapor. The atmospheric implications are discussed.

## Experimental Section

The samples used for the present experiments consisted of $NaNO_2$/NaCl salt mixtures coated with 1-oleoyl-2-palmitoyl-*sn*-glycero-3-phosphocholine (Sigma Aldrich, 97%). Pellets were prepared by mixing 0.35 g of NaCl (Aldrich 99%), 0.0014 g of $NaNO_2$ (Aldrich 99.99%) (0.4% w/w $NaNO_2$/NaCl), and $9.2 \times 10^{-4}$ g of OPPC. A Zeiss Evo LS 15 scanning electron microscope equipped with a Thermo Electron Corporation UltraDry Silicon Drift energy dispersive X-ray spectroscopy (EDS) detector was used to perform spectral imaging of salt powders to investigate the size distribution and the mixing of the salts. The procedure for coating the salt sample with OPPC and the diffuse reflection infrared Fourier transform spectroscopy (DRIFTS) apparatus are described in detail elsewhere.[51] The OPPC/$NaNO_2$/NaCl (0.35 g) was placed in the stainless steel holder of the DRIFTS vacuum chamber and compressed to form a solid pellet with a geometric surface area of 0.78 $cm^2$ and a volume of 0.16 $cm^3$.

The loss of nitrite ion and OPPC and the formation of products on the salt mixture were followed by using DRIFTS. In addition, matrix assisted laser desorption/ionization mass spectrometry (MALDI-MS) was used as described elsewhere[51] to confirm the identification of the products.

Photolysis of the sample was carried out with a high-pressure Xe arc lamp (Spectra Physics, Oriel 300 W, Model 6258 OF). An infrared filter consisting of continuously flowing water in a 10 cm long aluminum tube with quartz windows was attached to the arc lamp to prevent heating of the sample by IR radiation emitted by the lamp. A 1 mm Pyrex glass filter (<10% transmission at $\lambda < 290$ nm) was placed between the UV lamp and the quartz window to remove UV radiation that could photolyze OPPC itself. No loss of OPPC was observed during separate studies in which OPPC/NaCl was irradiated.

The relative lamp intensity as a function of wavelength was recorded with an Ocean Optics spectrometer (Model HR4000CG-UV-NIR). The total *absolute* intensity of the lamp integrated over the wavelength region from 300 to 400 nm was measured by using the photoisomerization of 2-nitrobenzaldehyde to 2-nitrosobenzoic acid, which is well-known to have a quantum

**TABLE 1: Assignment of the Infrared Bands Observed in the DRIFTS Spectra of OPPC/$NaNO_2$/NaCl before and after Photolysis**

| assignments | wavenumber ($cm^{-1}$) | vibrational mode | refs |
|---|---|---|---|
| $NaNO_2$ | 825 | ($\nu_1$) $NO_2$ bend | 59, 84 |
| $-N(CH_3)_3^+$ | 970 | $N-(CH_3)_3$ as def | 52, 59 |
| phosphate | 1095 | ($PO_2^-$) sym str | 52, 60 |
| phosphate | 1255 | ($PO_2^-$)as str | 52, 59, 60 |
| $NaNO_2$ | 1260 | ($\nu_2$) $NO_2$ as str | 59, 84 |
| R-$ONO_2$ | 1295 | $NO_2$ sym str | 59 |
| $NaNO_2$ | 1325 | ($\nu_3$) $NO_2$ sym str | 59, 84 |
| $NaNO_3$ | 1410−1350 | $NO_3$ as str | 59, 81 |
| $-N(CH_3)_3^+$ and $-CH_3$ | 1470 | $-CH_3$ bend | 59 |
| carboxylate | 1580 | CO str | 59 |
| R−$ONO_2$ | 1605 | $NO_2$ as str | 59, 85 |
| R−$ONO_2$ | 1628 | $NO_2$ as str | 59, 85 |
| hydrogen-bonded −COOH, aldehyde | 1708 | C═O str | |
| OPPC ester | 1735 | C═O str | 62 |
| non-hydrogen-bonded carboxylic acid −COOH | 1751 | C═O str | 59 |
| $-CH_2-$ | 2850 | $-CH_2-$ sym str | 52, 59 |
| $-CH_2-$ | 2919 | $-CH_2-$ as str | 52, 59 |
| $-CH_3$ | 2948 | $-CH_3$ as str | 52, 59 |
| C═C | 3008 | Vinyl C−H str | 52, 59 |
| hydrogen-bonded O−H | 3367 | O−H str | 59 |
| $H_2O$ | 3460 | H−O str (sym and as) | 59 |

yield for the rearrangement of 0.5.[57] Approximately 0.01 g of 2-nitrobenzaldehyde was pressed into a pellet with 0.5 g of NaCl and irradiated under the same conditions as the OPPC/$NaNO_2$/NaCl photolysis experiments. During irradiation, DRIFTS spectra were continuously recorded as a function of time and the peak at 1530 $cm^{-1}$, assigned to the asymmetric $NO_2$ stretch, was used to follow the disappearance of 2-nitrobenzaldehyde. The absorbed light intensity was calculated at various times and extrapolated to zero irradiation time in order to correct for absorption due to "internal filtering" as described by Pitts et al.[57] The relative lamp intensities as a function of wavelength were then converted to absolute intensities by determining the scaling factor by which they must be multiplied to obtain the total absolute intensity from 300 to 400 nm that was measured with the 2-nitrobenzaldehyde actinometer.

To generate the desired relative humidity over the sample, a flow of air was bubbled through Nanopure water (Barnstead, 18 MΩ·cm) and then diluted with a measured flow of dry air. During the photolysis experiments, the temperature of the sample increased by about 5 °C as measured by a thermocouple at the bottom of the salt pellet. After photolysis, it was necessary to pump the gases out and let the sample cool for ∼30 min to obtain consistent baselines.

Experiments were carried out with a flow of air (Ultrapure Air, Scott-Marrin, total hydrocarbons as $CH_4$ < 0.01 ppm; CO < 0.01 ppm; $NO_x$ < 0.001 ppm; $SO_2$ < 0.001 ppm) pumping over the sample during photolysis at a pressure of ∼750 Torr and a flow rate of 1.25 L $min^{-1}$ in the absence and presence of water vapor. Experiments in the presence of water vapor were carried out at 15% RH. Under these conditions, the salt remains in the solid state because at room temperature, NaCl crystals deliquesce at 75% RH and $NaNO_2$ at 66% RH.[58]

Infrared bands due to the formation of organic nitrates and carboxylates were observed upon photolysis of the OPPC/$NaNO_2$/NaCl mixture. To calibrate for the organic nitrates, DRIFTS spectra of mixtures of isosorbide-5-mononitrate (LKT Laboratories, Inc., >98%) with NaCl were recorded with total amounts from $1.3 \times 10^{-5}$ to $2.7 \times 10^{-4}$ g (0.004−0.08% w/w). Isosorbide-5-mononitrate was chosen because it has low volatility so that mixtures with NaCl can be made reliably. The infrared peaks due to the $-ONO_2$ group from the calibration mixtures were similar in intensity to those of organic nitrates observed in OPPC/$NaNO_2$/NaCl photolysis experiments. The absorption coefficient of the band at 1647 $cm^{-1}$ due to the asymmetric stretching vibration of the $NO_2$ group of the organic nitrate $RONO_2$ which was used for quantification is not expected to be very sensitive to the nature of the −R group. Carboxylates were quantified by comparison of the DRIFTS spectra of known mixtures of sodium palmitate (Aldrich, 99%) and isosorbide-5-mononitrate.

## Results and Discussion

**a. Characterization of Salt Samples.** The size distribution of OPPC/$NaNO_2$/NaCl particles formed by mechanical grinding was determined by visually examining SEM images of OPPC/$NaNO_2$/NaCl and measuring the diameter of individual particles. The average size was 1.8 $\mu$m (not taking into account particles 10 $\mu$m or larger, which represented less than 5% of the sample). The amount of OPPC added to the salt was sufficient to provide approximately 1 monolayer (ML) of coverage, if the OPPC was evenly distributed on cubic particles 1.8 $\mu$m on the edge.

Figure 1 (top) shows a typical SEM image of OPPC/$NaNO_2$/NaCl; for comparison, an SEM image of OPPC/NaCl is shown in the bottom part of Figure 1. Small granules appear to be attached to larger particles in the mixture containing nitrite, which we interpret to be granules of $NaNO_2$ on NaCl. This is supported by the data in Figure 2, which shows element maps for 5% $NaNO_2$/NaCl mixtures; the higher concentration of $NaNO_2$ in the sample used for EDS was necessary so that nitrogen and oxygen could be readily detected. It is seen that nitrogen and oxygen are colocated with Na and Cl, suggesting that the $NaNO_2$ largely coats the NaCl. In addition, small bright spots in the N and O images suggest small granules of pure $NaNO_2$ are attached to the larger NaCl particles. There is also a small area of the map where N and O can be seen but where there is no Na or Cl. This may be due to some $NaNO_2$ particles being dislodged from the NaCl during sample preparation.

**b. DRIFTS Spectra of Phospholipid-Coated $NaNO_2$/NaCl.** A typical DRIFTS spectrum of unreacted OPPC/NaCl is shown as the gray line in Figure 3. The spectrum was obtained by taking the ratio of a single beam spectrum of OPPC/NaCl to that of pure NaCl. Assignment of the bands is shown in Table 1.[59,60] Bands at ∼1255 and ∼1095 $cm^{-1}$ are observed for the phosphate asymmetric and symmetric stretches, respectively, and for the $N-(CH_3)_3^+$ head group at 970 and 1470 $cm^{-1}$. (The latter also has some contribution from $-CH_3$ deformation vibrations in the fatty acid chains.) The peak at 1735 $cm^{-1}$ is assigned to the carbonyl group of OPPC. Bands at 2948, 2919, and 2850 $cm^{-1}$ (inset in Figure 3) are observed for the C−H stretching modes of $-CH_3$ (2948 $cm^{-1}$) and $-CH_2-$ groups (2919 and 2850 $cm^{-1}$). The vinyl C−H stretch of OPPC at ∼3008 $cm^{-1}$ is also evident. The broad peak at ∼3460 $cm^{-1}$ is due to small amounts of adsorbed water. The black line in Figure 3 is the DRIFTS spectrum of unreacted OPPC/$NaNO_2$/NaCl. The addition of $NaNO_2$ to the salt results in additional bands at ∼1325 and 1260 $cm^{-1}$, and a weaker one at 825 $cm^{-1}$ due to $NO_2^-$.

**c. Photolysis of OPPC/$NaNO_2$/NaCl Mixtures.** Figure 4 shows spectra for OPPC/$NaNO_2$/NaCl during 90 min photolysis in air at selected times in the absence of added water vapor. Decreases in the 1200−1400 $cm^{-1}$ region and in the aliphatic and vinyl −CH bands (inset to Figure 4) were observed, as expected if nitrite ion photolyzes to generate oxidants that react

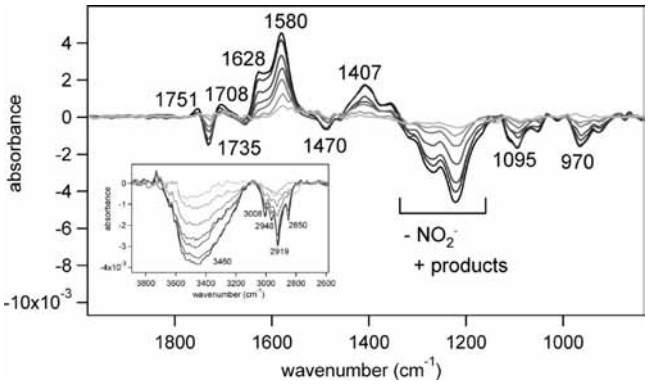


**Figure 4.** DRIFTS spectra of OPPC/$NaNO_2$/NaCl at ~0% RH in ultrapure air at increasing irradiation times (light gray to black, respectively) of 5, 10, 35, 50, 70, 80, and 90 min.

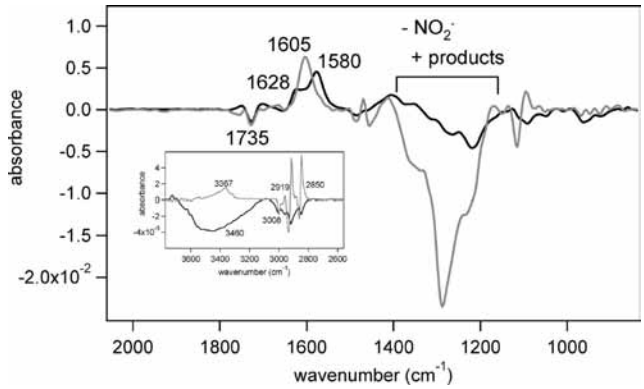


**Figure 5.** DRIFTS spectra of OPPC/$NaNO_2$/NaCl after 90 min of UV photolysis in ultrapure air at ~15% RH (gray line) and at ~0% RH (black line), respectively. The *y* axis is $\log(S_1/S_2)$, where $S_1$ and $S_2$ are the single beam spectra of OPPC/$NaNO_2$/NaCl before and after photolysis, respectively.

with the adsorbed organic. New bands due to product formation grow in at ~1628 and 1580 $cm^{-1}$ and in the region from ~1300 to 1450 $cm^{-1}$. (These product peaks and baseline shifts due to changes in the sample on exposure to water make it difficult to quantify the loss of nitrite using the 1260 $cm^{-1}$ band.) Weaker bands in the 1700−1750 $cm^{-1}$ region are also formed, but are masked in part by the simultaneous decrease in the OPPC carbonyl stretch at 1735 $cm^{-1}$. Small decreases were also observed for the phosphate symmetric stretch at ~1095 $cm^{-1}$ and for the $N-(CH_3)_3^+$ head group peaks at 970 $cm^{-1}$ and 1470 $cm^{-1}$.

Water is known to be strongly attracted by the zwitterionic head group of OPPC.[61,62] During photolysis under these dry conditions, the sample lost adsorbed water as shown by the decrease in the broad band at ~3460 $cm^{-1}$ for the H−O stretches of water (inset, Figure 4); a simultaneous decrease in the 1600−1650 $cm^{-1}$ water bend region is masked by the growth of the product peaks.

Figure 5 compares the final spectrum in Figure 4 after 90 min of UV photolysis to that when water vapor at 15% relative humidity is present during irradiation. It is clear that in the presence of water vapor there is a much greater extent of reaction, as evidenced by the larger decrease in the nitrite and C−H stretching regions (inset to Figure 5). Adsorbed water (3460 $cm^{-1}$) does not decrease significantly in the presence of water vapor. In addition, while small bands due to new product formation are still observed in the 1700−1750 and 1400 $cm^{-1}$ regions, the largest product peak is now at 1605 $cm^{-1}$.

The photolysis of nitrite generates $O^-$, reaction 4. In the absence of added water, which would convert it to OH, $O^-$ can

**SCHEME 1: Possible Reaction Mechanism for the Formation of the Carboxylate $RCO_2^-$ Ion, Which Dominates under Dry Conditions[a]**

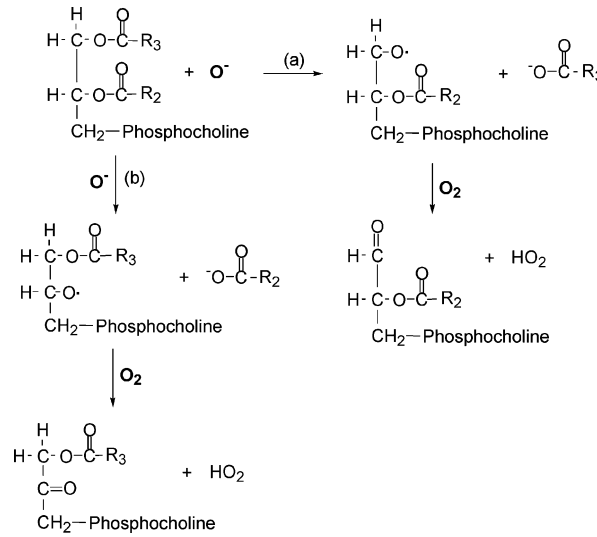


[a] $R_2$ is $(CH_2)_{14}CH_3$ and $R_3$ is $(CH_2)_7CH{=}CH(CH_2)_7CH_3$.

directly attack OPPC, leading to cleavage of a fatty acid at the ester linkage (Scheme 1). This will generate a carboxylate $RCO_2^-$ ion to which we assign the 1580 $cm^{-1}$ product peak seen in Figure 4.[59] Triacylglycerols undergo nucleophilic attack by $O^-$ to form carboxylate ions at rates that are not very sensitive to the nature of the fatty acid chain, e.g., palmitic versus oleic acid.[63,64] This reaction can proceed by two mechanisms, and similar reactions also occur in the presence of $OH^-$. In recent work, a peak at ~1580 $cm^{-1}$ was observed by DRIFTS in the ozonolysis of NaCl coated with OPPC followed by reaction with $NH_3$. The ozone reaction generated carboxylic acids that reacted with ammonia to form ammonium carboxylates.[51] Carboxylates also have weaker bands in the region around 1440−1400 $cm^{-1}$ assigned to a symmetric $COO^-$ stretch,[59] but these are difficult to differentiate since there are overlapping bands in this region of the IR.

Under "dry" conditions where no water was added to the carrier gas, there are still small amounts of adsorbed water on steps and edges of the salt.[23,65−73] More importantly, the zwitterionic head groups of the OPPC strongly attract water.[61,62] The loss of some of this water is readily observed during pumping on an OPPC-coated salt sample in the form of a broad negative band in the 3400 $cm^{-1}$ region similar to that in the inset in Figure 4. In the presence of adsorbed water, $O^-$ is rapidly converted to $OH^-$ and highly reactive OH radicals, reaction 3. This suggests that even in the absence of added water vapor, some fraction of the $O^-$ generated upon photolysis of nitrite will form OH radicals. Because adsorbed water under dry conditions is expected to be concentrated around the zwitterionic head group, the $-CH_2-$ groups at this end of the molecule will be most susceptible to oxidation by OH formed from $O^-$. Scheme 2 suggests that abstraction of a hydrogen from these groups leads to alkyl radicals, then to alkylperoxy radicals through reaction with $O_2$, and finally to organic nitrates via reaction with NO. Organic nitrates ($RONO_2$) have bands in the 1600−1650, 1270, and 840 $cm^{-1}$ regions due to the asymmetric and symmetric $NO_2$ stretches and the N−O stretching vibration, respectively.[59] We therefore assign the 1628 $cm^{-1}$ peak in Figure 4 from the reaction under dry conditions to organic nitrates of the types shown in Scheme 2. The peaks around 1270 and 840

**SCHEME 2: Proposed Mechanism for the Reaction of OH with the Head Group of OPPC under Dry Conditions**

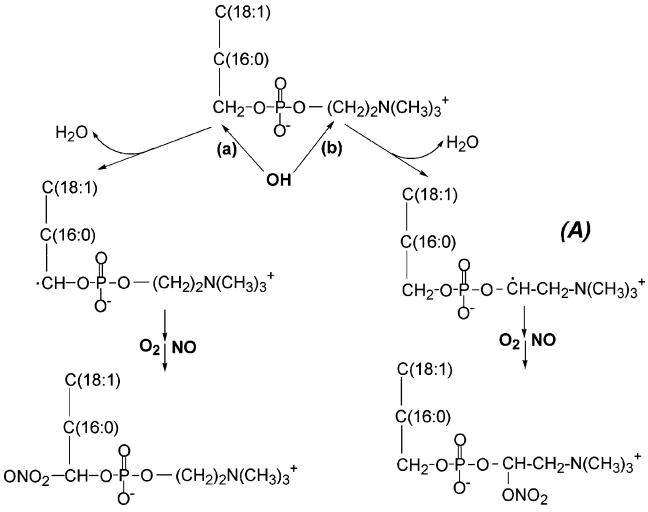


**SCHEME 3: Alternate Reaction Scheme for Product A in Scheme 2**

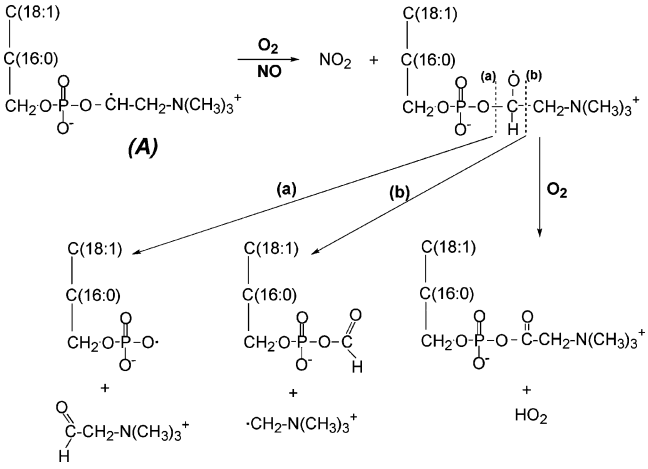


$cm^{-1}$ cannot be seen in the OPPC reaction due to the decrease in the overlapping nitrite bands.

An alternate fate of the $RO_2$ radical is its reaction with NO to generate an alkoxy radical, RO, which can form carbonyl compounds via reaction with $O_2$, or decompose to smaller fragments.[1] Scheme 3 summarizes just a few of these possibilities for the free radical **A** shown in Scheme 2. It is seen that scission of the head group at various points is expected, with the formation of new carbonyl groups adjacent to the phosphate and likely the $-N(CH_3)_3^+$ group as well. Such disruptions of the molecular integrity are likely responsible for the changes observed in the head group absorption bands in Figure 4, and for the appearance of new peaks in the ~1700 to 1750 $cm^{-1}$ region where C═O stretches occur but their position is sensitive to neighboring groups.[59] Other potential fates of the RO radical in addition to those shown in Scheme 3 include abstraction of a hydrogen atom to form an alcohol[74] or isomerization in which a hydrogen atom is internally transferred to form a hydroxyl alkyl radical.[1] Smith and co-workers[75] reported that the hydrogen abstraction pathway was likely occurring in the oxidation of liquid dioctyl sebacate particles but that isomerization was unimportant. While these reactions cannot be ruled out with certainty in the present system, the lack of MALDI-MS peaks at the expected masses suggests they are not major pathways.

With added water vapor, the $O^-$ will be converted via reaction 3 to OH and $OH^-$. It is therefore expected that under these conditions, oxidation by the hydroxyl radical will dominate relative to nucleophilic attack by $O^-$. Furthermore, because water will be more widely distributed rather than being concentrated near the head group, attack on the fatty acid chains including the C═C double bond is more likely. (Note that this also occurs to some extent in the absence of added water vapor.) The loss of the vinyl C−H group is expected, since OH adds rapidly to C═C double bonds and, in the presence of air, an alkylperoxy free radical $RO_2$ is formed (Scheme 4). Nitric oxide formed simultaneously in the nitrite photolysis reacts with $RO_2$ to either form an organic hydroxynitrate **B** or an alkoxy radical **C** in Scheme 4. Subsequent reactions convert **C** into the phospholipid aldehyde **D**, and nonanal. Because a flow of air is being pumped through the sample during irradiation, gaseous products such as nonanal will be lost, resulting in negative peaks in the C−H region from ~2800 to 3000 $cm^{-1}$, as observed (Figures 4 and 5).

The formation of an organic nitrate is consistent with the formation of the peak at 1605 $cm^{-1}$. The fact that this peak appears at a different position from that formed under dry conditions reflects different neighboring groups[59] due to the different locations of primary attack of OH and hence of addition of the nitrate group, i.e., around the head group in the absence of added water vapor and at the fatty acid chains in its presence. The small peak at 3367 $cm^{-1}$ (Figure 5) is assigned to the O−H stretch of the alcohol group.[59]

The formation of the organic nitrate **B** (Scheme 4) was confirmed by MALDI-MS. At 15% RH, a peak at 862 amu corresponding to the sodium adduct of **B** (839 amu) was observed after photolysis. Additional peaks observed at 651 and 673 amu are the $[M + H]^+$ and $[M + Na]^+$ peaks of the phospholipid aldehyde **D**. These are essentially the same as those observed in earlier studies at 52% RH,[56] and hence the spectra are not shown here. Although quantitative measurements of the product yields from the MALDI-MS are not possible due to varying signal intensities from the highly variable matrix-to-analyte ratios across the sample,[76−78] the relative peak intensities indicate that the product yields increase with increasing water vapor concentration.

Another MALDI-MS peak was observed at 728 amu. The assignment of this peak remains uncertain; one possibility is an organic nitrate formed by abstraction of an allylic hydrogen, a process that has been observed as a significant pathway in the reaction of $O^-$ with unsaturated organics.[63] For example, abstraction of the allylic C−H closest to the backbone followed by formation of an organic nitrate at this position and then oxidation of the double bond to a carboxylic acid would give product **E** in Scheme 5 that has a molecular weight of 727 amu. The $[M + H]^+$ peak would then appear at 728.

It should be noted that attack at the C═C bond may also occur to some extent under dry conditions, but the smaller extent of reaction precluded MALDI-MS confirmation. The differential shape of the peaks around 2919 and 2850 $cm^{-1}$, corresponding to $-CH_2-$ stretches in the 15% RH case, suggests that substituents on the products shift the peaks in that region. The formation of new carbonyl groups is again reflected in the product peaks in the 1700−1750 $cm^{-1}$ region.

The greater extent of reaction for photolysis experiments in the presence of water vapor is likely due to the effects of increased ion mobility. A number of studies have observed that the presence of even relatively small amounts of water

**SCHEME 4: Partial Reaction Mechanism To Form Products B and D Observed by MALDI-MS**

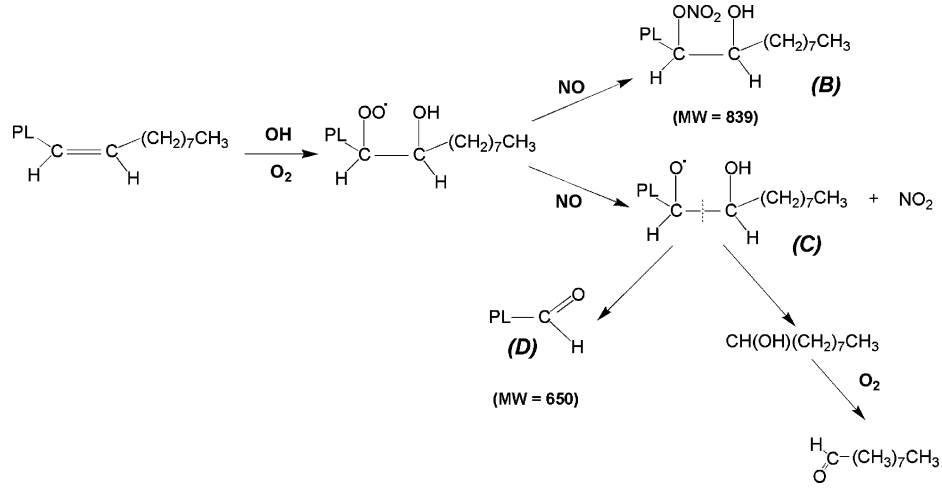


**SCHEME 5: Potential Formation Mechanism for the Peak at 728 amu Observed in MALDI-MS Analysis**

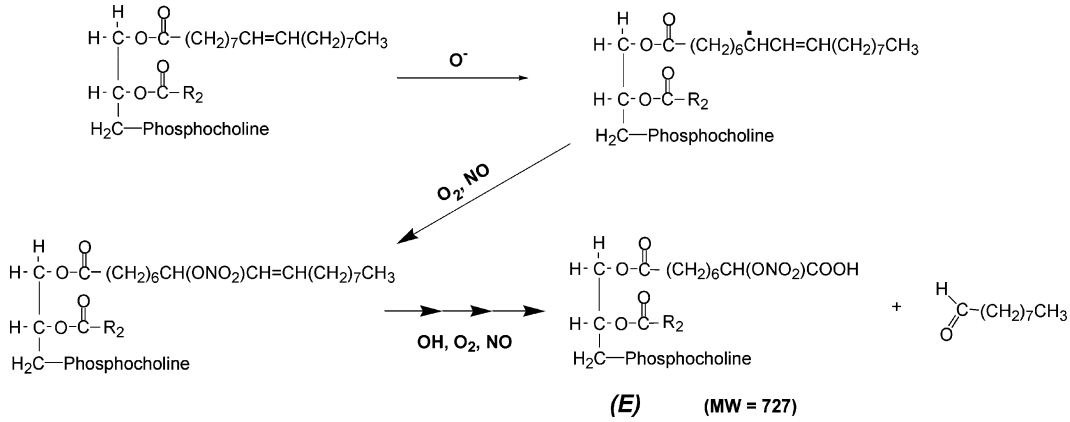


vapor aids in the movement of ions on salt surfaces.[23,68−70,73,79−81] In the case of an NaCl surface reacted with $HNO_3$, for example, exposure to water vapor allows the nitrate ions to segregate into separate microcrystallites on a fresh NaCl surface.[79] In the present case, $NO_2^-$ photolyzes to $O^-$, which in the presence of water forms $OH + OH^-$, reaction 3 above. Thus, the surface will be converted from $NaNO_2$ to NaOH. This will ultimately lead to surface passivation so that $O^-$ formed upon photolysis of $NO_2^-$ in the underlying layers is more likely to recombine with NO to regenerate $NO_2^-$, effectively quenching the photochemistry. The presence of water vapor keeps the surface ions mobile so that $NO_2^-$ is continuously exposed at the surface, leading to greater extents of reaction as the water vapor concentration increases.

**d. Rate of Photolysis of $NO_2^-$ and Product Yields.** The photolysis rate constant for $NO_2^-$ to generate OH was determined by using eq I,

$$k_p\,(s^{-1}) = \sum_{\lambda>290\text{ nm}} I(\lambda)\,\sigma(\lambda)\,\Phi_{OH}(\lambda)\,\Delta\lambda \qquad \text{(I)}$$

where $I(\lambda)$ is the absolute light intensity (photons $cm^{-2}$ $s^{-1}$ $nm^{-1}$), $\sigma(\lambda)$ is the absorption cross section ($cm^2$ $molecule^{-1}$) in aqueous solutions,[2] and $\Phi_{OH}(\lambda)$ is the quantum yield of OH formation from $NO_2^-$ photolysis in aqueous solutions.[8,17,28,29] The calculation was carried out by using $\Delta\lambda = 0.5$ nm intervals from 290 to 400 nm.

The photoisomerization of 2-nitrobenzaldehyde measured in four separate experiments gave a value for the total integrated absolute intensity over the 300−400 nm region of $(1.4 \pm 0.4) \times 10^{17}$ photons $s^{-1}$ ($2\sigma$). This was used to convert the measured relative intensities as a function of wavelength to absolute intensities as a function of wavelength, $I(\lambda)$. By using eq I, $\sigma$ from Zuo and Deng,[2] and $\Phi_{OH}$ from Chu and Anastasio,[8] the photolysis rate constant to generate OH, $k_p$, was calculated to be $(2.5 \pm 1.0) \times 10^{-5}$ $s^{-1}$ ($2\sigma$).

An upper estimate to the rate of OH production (or $O^-$ in the absence of water) should then be given by $d(OH)/dt = k_p\{NO_2^-\}$, where $\{NO_2^-\}$ is the initial number of nitrite ions in the pellet and it is assumed that all ions are equally irradiated. This is calculated to be $(3.0 \pm 1.2) \times 10^{14}$ molecules $O^-$/OH $s^{-1}$ ($2\sigma$), which over an integration time of 90 min gives a total calculated number of $O^-$/OH generated of $(1.6 \pm 0.6) \times 10^{18}$ radicals. This estimate incorporates literature values[8] of the quantum yields for OH from nitrite photolysis in solution at room temperature measured under conditions where essentially all of the $O^-$ is converted to OH, which was captured by an organic trapping agent. The reported quantum yields vary from 2% to 7% over the wavelength range used in the present studies, with an average of 3% when weighted by our relative lamp intensities.

However, the present situation, an organic coating on a solid salt mixture, is quite different than an aqueous solution. The hydroxyl radical is known to undergo a competing reaction with $NO_2^-$ in solution at a rate that is essentially diffusion-controlled,[17]

$$OH + NO_2^- \rightarrow NO_2 + OH^- \quad (5)$$

and a rapid reaction is also expected in the solid. This suggests that only the OH generated at or very near the surface of the salt that is in contact with the organic coating will have an opportunity to react with OPPC, the rest being trapped by reaction 5 with nitrite. Under dry conditions where water is clustered around the head group, abstraction of a hydrogen atom from a C−H bond is expected to dominate the OPPC oxidation (Scheme 2). Rate constants for abstraction of a hydrogen atom from a C−H bond are about 1 to 2 orders of magnitude below diffusion-controlled. This suggests that even under the unrealistic conditions of equal accessibility of nitrite and OPPC, only 1−10% of the OH that is generated will react with the alkyl C−H groups in OPPC, while the majority will further oxidize nitrite ions to form gaseous $NO_2$ and $OH^-$.

The reaction of OH with the double bond is much faster, approaching that of reaction 5. This suggests that at higher RH under ideal conditions of equal accessibility of the double bond and $NO_2^-$, an upper limit of 50% of the OH could oxidize OPPC. An additional factor that depends on RH is surface passivation, as discussed earlier. The formation of NaOH during photolysis will form an unreactive layer between the OPPC and the underlying $NaNO_2$, effectively quenching the organic oxidation. This effect is expected to decrease with increasing RH since water enhances ion mobility on the surface.

The measured products formed in 90 min are consistent with this mechanism. Thus, in the absence of water vapor, the number of organic nitrate molecules was $(2.1 \pm 0.3) \times 10^{16}$ molecules, based on DRIFTS calibrations of known isosorbide-5-mononitrate−NaCl mixtures. At 0% RH, carboxylate was also observed (Figure 4). DRIFTS spectra of known mixtures of isosorbide mononitrate and sodium palmitate showed that the 1580 $cm^{-1}$ peak at 90 min in Figure 4 represents $(7.5 \pm 1.1) \times 10^{15}$ $RCO_2^-$. The total number of $RONO_2 + RCO_2^-$ product molecules after 90 min is therefore $(2.9 \pm 0.6) \times 10^{16}$ molecules, which represents 1.8% of the calculated $OH/O^-$ production. Although there are some aldehydes and ketones formed as well (Figures 4 and 5), these are relatively small and will not substantially increase this estimate.

At 15% RH, organic nitrates are still the major product, with $(5.6 \pm 0.8) \times 10^{16}$ molecules formed after 90 min. This represents 3.5% of the calculated OH generated. In earlier studies at 52% RH,[56] $(2.1 \pm 0.5) \times 10^{17}$ $RONO_2$ were measured after 90 min photolysis, corresponding to 13% of the OH formed. The MALDI spectra support reaction of OH in part with the double bond (Scheme 4) at 15% and 52% RH. This is consistent with greater trapping of the OH at higher water vapor concentrations by OPPC compared to reaction with $NO_2^-$. In addition, surface passivation will be less severe due to enhanced mobility of the surface ions caused by the presence of water. In short, the product yields and their trends with RH are both consistent with the known chemistry and photochemistry in this system.

## Atmospheric Implications

This work conclusively demonstrates that oxidation of an organic coating on particles can occur even in the absence of gas phase oxidants if reactive species such as OH can be generated at the interface. While extrapolation to atmospheric conditions should be approached with caution, the increasing trend in the yield of organic products with RH suggests that the present results are lower limits for the atmospheric situation where particles containing nitrite are typically aqueous. In addition, this chemistry is likely to be important for nitrate ions as well, which also generate OH via reactions 2a and 3.

Ground-based measurements of the gas and aerosol phases in Marseille[82] indicated that ∼65% of the inorganic nitrite was present as HONO in the gas phase and ∼35% as $NO_2^-$ in wet aerosols. Peak aerosol nitrite concentrations ranged from 0.6 to 1.0 $\mu g\ m^{-3}$, and the corresponding range for peak aerosol nitrate ranged from 2 to 8 $\mu g\ m^{-3}$. By using the known absorption cross sections and quantum yields for nitrite and nitrate photolysis, the photolysis rate constants at a solar zenith angle of 0° on July 1 were calculated to be $k_p(NO_2^-) = 2.6 \times 10^{-5}\ s^{-1}$ and $k_p(NO_3^-) = 3.9 \times 10^{-7}\ s^{-1}$. Even with nitrite concentrations an order of magnitude smaller than those for nitrate, the rate of generation of OH by $NO_2^-$ will be 11 times greater than that from $NO_3^-$ under the peak conditions reported for Marseille.[82]

The photolysis rate constant calculated for nitrite for an overhead sun implies a lifetime with respect to photolysis of 11 h. Nitrite is also oxidized by $O_3$ with a rate constant[83] of $3.7 \times 10^5\ L\ mol^{-1}\ s^{-1}$, and this reaction also generates OH radicals. At 50 ppb $O_3$ and with an $O_3$ Henry's law constant[1] of $1.3 \times 10^{-3}\ mol\ L^{-1}\ atm^{-1}$, the lifetime of $NO_2^-$ with respect to $O_3$ is also about 11 h. Thus, most of the nitrite will react over a day to form OH. Assuming that all of the OH reacts with organics in or on the particles, equimolar amounts of new organic products would be formed. Perhaps more important than the amount formed is that some of the organic products will be in the form of organic nitrates. This represents a possible mechanism for temporary sequestration of oxides of nitrogen. The organic nitrates formed are likely to be multifunctional, and if they contain carbonyl groups, for example, may ultimately photolyze and undergo secondary reactions to release nitrogen oxides back into the atmosphere downwind of their point of formation. Oxidation of the organic nitrates, e.g., by OH, will also contribute to this subsequent release of $NO_y$.

Nitrite is also present in snowpacks where its photolysis is believed to be a significant source of $NO_x$.[8,16] Although it is expected to be a smaller source of OH than photolysis of $H_2O_2$,[8] the present studies suggest that organic nitrates may also be formed from this chemistry. As discussed above, this could serve as a temporary reservoir of oxides of nitrogen in the snowpack.

**Acknowledgment.** It is an honor to dedicate this paper to Professor R. Benny Gerber, a true scholar and gentleman whose work has contributed immensely to molecular-level understanding of fundamental chemical processes. Most recently, his applications of state-of-the-art theory to systems of atmospheric interest and the intertwining of theory and experiments to provide wonderful insights that could not have been provided by either approach alone have yielded unparalleled advances in understanding complex atmospheric systems. We look forward to many more such innovative contributions and continuing exciting and productive collaborations in the future. We are grateful to the National Science Foundation (Grant no. ATM-0423804) for support of this work, and to Dr. John Greaves for assistance with the MALDI-MS. The authors thank the staff of the Carl Zeiss

Center for Excellence in Electron Microscopy at the University of California, Irvine for assistance and access to the facilities.

## References and Notes

(1) Finlayson-Pitts, B. J.; Pitts, J. N., Jr. *Chemistry of the Upper and Lower Atmosphere−Theory, Experiments, and Applications*; Academic Press: San Diego, CA, 2000.
(2) Zuo, Y. G.; Deng, Y. W. *Chemosphere* **1998**, *36*, 181.
(3) Anastasio, C.; Galbavy, E. S.; Hutterli, M. A.; Burkhart, J. F.; Friel, D. K. *Atmos. Environ.* **2007**, *41*, 5110.
(4) Chu, L.; Anastasio, C. *J. Phys. Chem.* **2003**, *107*, 9594.
(5) Galbavy, E. S.; Anastasio, C.; Lefer, B.; Hall, S. *Atmos. Environ.* **2007**, *41*, 5091.
(6) Galbavy, E. S.; Anastasio, C.; Lefer, B. L.; Hall, S. R. *Atmos. Environ.* **2007**, *41*, 5077.
(7) Anastasio, C.; McGregor, K. G. *Atmos. Environ.* **2001**, *35*, 1079.
(8) Chu, L.; Anastasio, C. *Environ. Sci. Technol.* **2007**, *41*, 3626.
(9) Grannas, A. M.; Jones, A. E.; Dibb, J.; Ammann, M.; Anastasio, C.; Beine, H. J.; Bergin, M.; Bottenheim, J.; Boxe, C. S.; Carver, G.; Chen, G.; Crawford, J. H.; Domine, F.; Frey, M. M.; Guzman, M. I.; Heard, D. E.; Helmig, D.; Hoffmann, M. R.; Honrath, R. E.; Huey, L. G.; Hutterli, M.; Jacobi, H. W.; Klan, P.; Lefer, B.; McConnell, J.; Plane, J.; Sander, R.; Savarino, J.; Shepson, P. B.; Simpson, W. R.; Sodeau, J. R.; von Glasow, R.; Weller, R.; Wolff, E. W.; Zhu, T. *Atmos. Chem. Phys.* **2007**, *7*, 4329.
(10) Honrath, R. E.; Guo, S.; Peterson, M. C.; Dziobak, M. P.; Dibb, J. E.; Arsenault, M. A. *J. Geophys. Res.* **2000**, *105*, 24183.
(11) Honrath, R. E.; Peterson, M. C.; Dziobak, M. P.; Dibb, J. E.; Arsenault, M. A.; Green, S. A. *Geophys. Res. Lett.* **2000**, *27*, 2237.
(12) Honrath, R. E.; Peterson, M. C.; Guo, S.; Dibb, J. E.; Shepson, P. B.; Campbell, B. *Geophys. Res. Lett.* **1999**, *26*, 695.
(13) Dubowksi, Y.; Colussi, A. J.; Hoffmann, M. R. *J. Phys. Chem. A* **2001**, *105*, 4928.
(14) Dubowski, Y.; Colussi, A. L.; Boxe, C.; Hoffmann, M. R. *J. Phys. Chem. A* **2002**, *106*, 6967.
(15) Boxe, C. S.; Colussi, A. J.; Hoffman, M. R.; Tan, D.; Mastromarino, J.; Case, A. T.; Sandholm, S. T.; Davis, D. D. *J. Phys. Chem. A* **2003**, *107*, 11409.
(16) Jones, A. E.; Wolff, E. W.; Salmon, R. A.; Bauguitte, S. J. B.; Roscoe, H. K.; Anderson, P. S.; Ames, D.; Clemitshaw, K. C.; Fleming, Z. L.; Bloss, W. J.; Heard, D. E.; Lee, J. D.; Read, K. A.; Hamer, P.; Shallcross, D. E.; Jackson, A. V.; Walker, S. L.; Lewis, A. C.; Mills, G. P.; Plane, J. M. C.; Saiz-Lopez, A.; Sturges, W. T.; Worton, D. R. *Atmos. Chem. Phys.* **2008**, *8*, 3789.
(17) Mack, J.; Bolton, J. R. *J. Photochem. Photobiol. A* **1999**, *128*, 1.
(18) Finlayson-Pitts, B. J.; Wingen, L. M.; Sumner, A. L.; Syomin, D.; Ramazan, K. A. *Phys. Chem. Chem. Phys.* **2003**, *5*, 223.
(19) Syomin, D. A.; Finlayson-Pitts, B. J. *Phys. Chem. Chem. Phys.* **2003**, *5*, 5236.
(20) Stutz, J.; Alicke, B.; Ackermann, R.; Geyer, A.; Wang, S. H.; White, A. B.; Williams, E. J.; Spicer, C. W.; Fast, J. D. *J. Geophys. Res* **2004**, *110,* DOI:10.1029/2003JD004135.
(21) Woodcock, A. H. *J. Meteorol.* **1953**, *10*, 362.
(22) Lewis, E. R.; Schwartz, S. E. *Sea Salt Aerosol Production: Mechanisms, Methods, Measurements and Models. A Critical Review*; American Geophysical Union: Washington, D.C., 2005; Vol. 152.
(23) Finlayson-Pitts, B. J. *Chem. Rev.* **2003**, *103*, 4801.
(24) Rossi, M. J. *Chem. Rev.* **2003**, *103*, 4823.
(25) Schroeder, W. H.; Urone, P. *Environ. Sci. Technol.* **1974**, *8*, 756.
(26) Finlayson-Pitts, B. J. *Nature* **1983**, *306*, 676.
(27) Daniels, M.; Meyers, R. V.; Belardo, E. V. *J. Phys. Chem.* **1968**, *72*, 389.
(28) Zellner, R.; Exner, M.; Herrmann, H. *J. Atmos. Chem.* **1990**, *10*, 411.
(29) Herrmann, H. *Phys. Chem. Chem. Phys.* **2007**, *9*, 3935.
(30) Buxton, G. V.; Greenstock, C. L.; Helman, W. P.; Ross, A. B. *J. Phys. Chem. Ref. Data* **1988**, *17*, 513.
(31) Fischer, M.; Warneck, P. *J. Phys. Chem.* **1996**, *100*, 18749.
(32) Arakaki, T.; Miyake, T.; Hirakawa, T.; Sakugawa, H. *Environ. Sci. Technol.* **1999**, *33*, 2561.
(33) Zafiriou, O. C. *J. Geophys. Res.* **1974**, *79*, 4491.
(34) Zafiriou, O. C.; Bonneau, R. *Photochem. Photobiol.* **1987**, *45*, 723.
(35) Alif, A.; Boule, P. *J. Photochem. Photobiol. A* **1991**, *59*, 357.
(36) Mopper, K.; Zhou, X. L. *Science* **1990**, *250*, 661.
(37) Anastasio, C.; Martin, S. T. Atmospheric nanoparticles. In. *Nanoparticles and the Environment* **2001**, *44*, 293.
(38) Pöschl, U. *Angew. Chem., Int. Ed.* **2005**, *44*, 7520.
(39) Rudich, Y.; Donahue, N. M.; Mentel, T. F. *Annu. Rev. Phys. Chem.* **2007**, *58*, 321.
(40) Rudich, Y. *Chem. Rev.* **2003**, *103*, 5097.
(41) Ellison, G. B.; Tuck, A. F.; Vaida, V. *J. Geophys. Res.* **1999**, *104*, 11633.
(42) Blanchard, D. C. *Science* **1964**, *146*, 396.
(43) Blanchard, D. C. *J. Rech. Atmos.* **1974**, *8*, 529.
(44) Gagosian, R. B.; Peltzer, E. T.; Zafiriou, O. C. *Nature* **1981**, *291*, 312.
(45) Marty, J. C.; Saliot, A.; Buatmenard, P.; Chesselet, R.; Hunter, K. A. *J. Geophys. Res.* **1979**, *84*, 5707.
(46) Tervahattu, H.; Hartonen, K.; Kerminen, V.-M.; Kupiainen, K.; Aarnio, P.; Koskentalo, T.; Tuck, A. F.; Vaida, V. *J. Geophys. Res.* **2002**, *107,* DOI:10.109/2000JD000282..
(47) Tervahattu, H.; Juhanoja, J.; Kupiainen, K. *J. Geophys. Res.* **2002**, *107*, DOI:10.1029/2001JD001403.
(48) Tervahattu, H.; Juhanoja, J.; Vaida, V.; Tuck, A. F.; Niemi, J. V.; Kupiainen, K.; Kulmala, M.; Vehkamaki, H. *J. Geophys. Res., [Atmos.]* **2005**, *110*, DOI:10.1029/2004JD005400.
(49) Sumner, A. L.; Shepson, P. B. *Nature* **1999**, *398*, 230.
(50) Sumner, A. L.; Shepson, P. B.; Grannas, A. M.; Bottenheim, J. W.; Anlauf, K. G.; Worthy, D.; Schroeder, W. H.; Steffen, A.; Dominé, F.; Perrier, S.; Houdier, S. *Atmos. Environ.* **2002**, *36*, 2553.
(51) Karagulian, F.; Lea, A. S.; Dilbeck, C. W.; Finlayson-Pitts, B. J. *Phys. Chem. Chem. Phys.* **2008**, *10*, 528.
(52) Finlayson-Pitts, B. J.; Sweetman, L. L.; Weissbart, B. *Toxicol. Appl. Pharmacol.* **1987**, *89*, 438.
(53) Lai, C. C.; Finlayson-Pitts, B. J.; Willis, W. V. *Chem. Res. Toxicol.* **1990**, *3*, 517.
(54) Lai, C. C.; Yang, S.; Finlayson-Pitts, B. J. *Langmuir* **1994**, *10*, 4637.
(55) Wadia, Y.; Tobias, D. J.; Stafford, R.; Finlayson-Pitts, B. J. *Langmuir* **2000**, *16*, 9321.
(56) Karagulian, F.; Dilbeck, C. W.; Finlayson-Pitts, B. J. *J. Am. Chem. Soc.* **2008**, *130*, 11272.
(57) Pitts, J. N., Jr.; Wan, J. K. S.; Schuck, E. A. *J. Am. Chem. Soc.* **1964**, *86*, 3606.
(58) Twomey, S. *J. Appl. Phys.* **1953**, *24*, 1099.
(59) Socrates, G. *Infrared and Raman Characteristic Group Frequencies*; John Wiley & Sons: New York, 2001.
(60) Arrondo, J. L. R.; Goni, F. M.; Macarulla, J. M. *Biochim. Biophys. Acta* **1984**, *794*, 165.
(61) Fingeli, U. P.; Gunthard, H. H. Infrared membrane spectroscopy. In *Membrane Spectroscopy*; Springer: Berlin, Germany, 1981; p 270.
(62) Hübner, W.; Blume, A. *Chem. Phys. Lipids* **1998**, *96*, 99.
(63) Cheung, M.; Young, A. B.; Harrison, A. G. *J. Am. Soc. Mass Spectrom.* **1994**, *5*, 553.
(64) Johlman, C. L.; Wilkins, C. L. *J. Am. Chem. Soc.* **1985**, *107*, 327.
(65) Cabrera-Sanfelix, P.; Portal, D. S.; Verdaguer, A.; Darling, G. R.; Salmeron, M.; Arnau, A. *J. Phys. Chem. C* **2007**, *111*, 8000.
(66) Dai, D. J.; Peters, S. J.; Ewing, G. E. *J. Phys. Chem.* **1995**, *99*, 10299.
(67) Foster, M. C.; Ewing, G. E. *J. Chem. Phys.* **2000**, *112*, 6817.
(68) Ghosal, S.; Hemminger, J. C. *J. Phys. Chem. A* **1999**, *103*, 4777.
(69) Ghosal, S.; Hemminger, J. C. *J. Phys. Chem. B* **2004**, *108*, 14102.
(70) Luna, M.; Rieutord, F.; Melman, N. A.; Dai, Q.; Salmeron, M. *J. Phys. Chem. A* **1998**, *102*, 6793.
(71) Peters, S. J.; Ewing, G. E. *Langmuir* **1997**, *13*, 6345.
(72) Peters, S. J.; Ewing, G. E. *J. Phys. Chem. B* **1997**, *101*, 10880.
(73) Verdaguer, A.; Sacha, G. M.; Luna, M.; Frank Ogletree, D.; Salmeron, M. *J. Chem. Phys.* **2005**, *123*, 8.
(74) Avila, D. V.; Brown, C. E.; Ingold, K. U.; Lusztyk, J. *J. Am. Chem. Soc.* **1993**, *115*, 466.
(75) Hearn, J. D.; Renbaum, L. H.; Wang, X.; Smith, G. D. *Phys. Chem. Chem. Phys.* **2007**, *9*, 4803.
(76) Cohen, L. H.; Gusev, A. I. *Anal. Bioanal. Chem.* **2002**, *373*, 571.
(77) Harvey, D. J. *Mass Spectrom. Rev.* **1999**, *18*, 349.
(78) Petkovic, M.; Schiller, J.; Muller, J.; Muller, M.; Arnold, K.; Arnhold, J. *Analyst* **2001**, *126*, 1042.
(79) Allen, H. C.; Laux, J. M.; Vogt, R.; Finlayson-Pitts, B. J.; Hemminger, J. C. *J. Phys. Chem.* **1996**, *100*, 6371.
(80) Ghosal, S.; Vergaguer, A.; Hemminger, J. C.; Salmeron, M. *J. Phys Chem. B* **2005**, *109*, 4744.
(81) Vogt, R.; Finlayson-Pitts, B. J. *J. Phys. Chem.* **1994**, *98*, 3747.
(82) Acker, K.; Moller, D.; Auel, R.; Wieprecht, W.; Kalass, D. *Atmos. Res.* **2005**, *74*, 507.
(83) Hoigné, J.; Bader, H.; Haag, W. R.; Staehelin, J. *Water Res.* **1985**, *19*, 993.
(84) Hammad, T. M. *Ann. Phys.* **2002**, *11*, 435.
(85) Chen, X. H.; Hulbert, D.; Shepson, P. B. *J. Geophys. Res., [Atmos.]* **1998**, *103*, 25563.

JP808419G